PCCP

ROYAL SOCIETY OF CHEMISTRY

PAPER

View Article Online
View Journal | View Issue

Cite this: *Phys. Chem. Chem. Phys.*, 2023, **25**, 8497

Real-time observation of the Woodward–Hoffmann rule for 1,3-cyclohexadiene by femtosecond soft X-ray transient absorption†

Taro Sekikawa, *[a] Nariyuki Saito,[b] Yutaro Kurimoto,[a] Nobuhisa Ishii,[c] Tomoya Mizuno,[b] Teruto Kanai,[b] Jiro Itatani,[b] Kenichiro Saita[d] and Tetsuya Taketsugu[de]

The stereochemistry of pericyclic reactions is explained by orbital symmetry conservation, referred to as the Woodward–Hoffmann (WH) rule. Although this rule has been verified using the structures of reactants and products, the temporal evolution of the orbital symmetry during the reaction has not been clarified. Herein, we used femtosecond soft X-ray transient absorption spectroscopy to elucidate the thermal pericyclic reaction of 1,3-cyclohexadiene (CHD) molecules, *i.e.*, their isomerization to 1,3,5-hexatriene. In the present experimental scheme, the ring-opening reaction is driven by the thermal vibrational energy induced by photoexcitation to the Rydberg states at 6.2 eV and subsequent femtosecond relaxation to the ground state of CHD molecules. The direction of the ring opening, which can be conrotatory or disrotatory, was the primary focus, and the WH rule predicts the disrotatory pathway in the thermal process. We observed the shifts in K-edge absorption of the carbon atom from the 1s orbital to vacant molecular orbitals around 285 eV at a delay between 340 and 600 fs. Furthermore, a theoretical investigation predicts that the shifts depend on the molecular structures along the reaction pathways and the observed shifts in induced absorption are attributed to the structural change in the disrotatory pathway. This confirms that the orbital symmetry is dynamically conserved in the ring-opening reaction of CHD molecules as predicted using the WH rule.

Received 10th November 2022,
Accepted 15th February 2023

DOI: 10.1039/d2cp05268g

rsc.li/pccp

1. Introduction

Electrocyclic reactions occur in various biosynthetic and biomimetic processes.[1] The photo-induced ring-opening reaction of cyclic 1,3-cyclohexadiene (CHD) to straight-chain 1,3,5-hexatriene (HT) (Fig. 1a) is one of the simplest electrocyclic reactions,[2,3] a kind of pericyclic reaction, and is the prototype reaction for understanding the nature of more complicated biosynthetic processes. One interesting feature of electrocyclic reactions is stereoselectivity under thermal and photochemical conditions, which is determined from the symmetry of molecular orbitals (MOs). The symmetry of the MOs before and after the reaction is preserved,[4] which is called the Woodward–Hoffmann (WH) rule.[5] The prediction of stereoselectivity in chemical reactions is very important in the synthesis of organic materials.

Fig. 1b shows that the ring-opening reaction in CHD involves a disrotatory and a conrotatory pathway. The disrotatory pathway is the thermal process, where the two CH_2 groups rotate in opposite directions while conserving the symmetry plane; contrarily, the conrotatory pathway is the photoexcitation process, where the two CH_2 groups rotate in the same direction while conserving the symmetry axis. The selectivity of the two pathways can be understood intuitively by considering the correlation diagram of the C–C σ bonding/antibonding orbitals and four π orbitals of CHD and the six π orbitals of HT shown in Fig. 1c. In the disrotatory pathway, the MOs of CHD are fully occupied up to π_2 orbitals and the symmetry of each MO is classified as symmetric (S) and antisymmetric (A) with respect to the mirror image operation. Before and after the ring-opening reaction, the symmetry of the occupied MOs is conserved because both CHD and HT have two S and one A orbitals. Hence, the thermal reactions proceed through the disrotatory pathway. On the other hand, in the conrotatory pathway,

[a] *Department of Applied Physics, Faculty of Engineering, Hokkaido University, Sapporo 060-8628, Japan. E-mail: sekikawa@eng.hokudai.ac.jp*
[b] *Institute for Solid State Physics, University of Tokyo, Kashiwa 277-8581, Japan*
[c] *Kansai Photon Science Institute, National Institutes for Quantum and Radiological Science and Technology, Kizugawa 619-0215, Japan*
[d] *Department of Chemistry, Faculty of Science, Hokkaido University, Sapporo 060-0810, Japan*
[e] *Institute for Chemical Reaction Design and Discovery (WPI-ICReDD), Hokkaido University, Sapporo 001-0021, Japan*

† Electronic supplementary information (ESI) available. See DOI: https://doi.org/10.1039/d2cp05268g

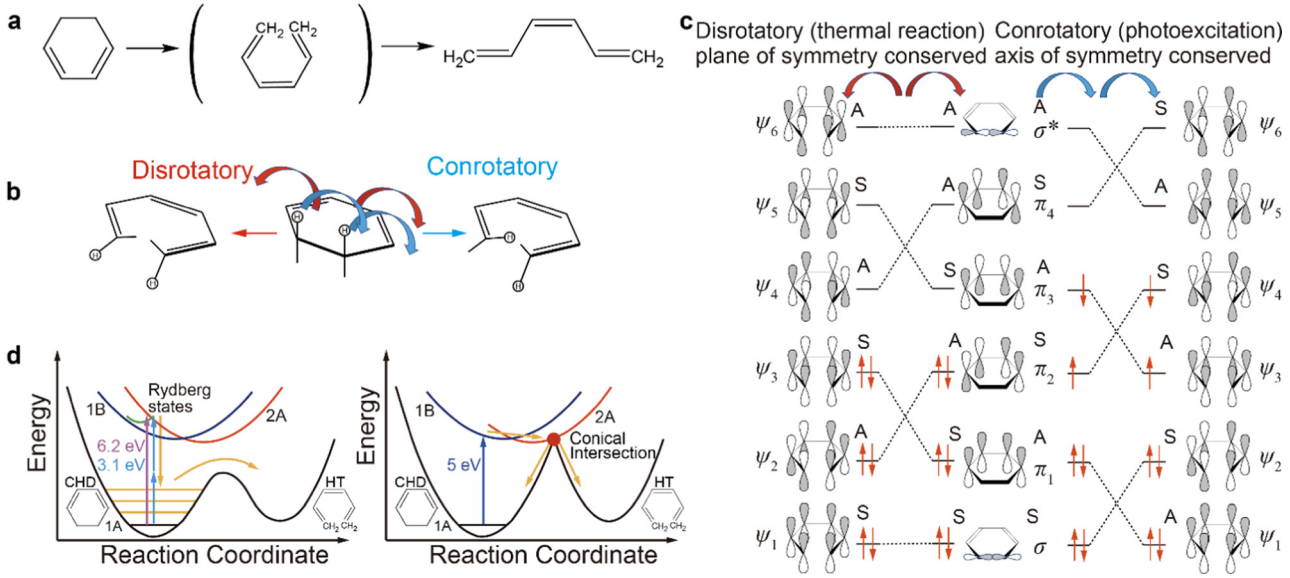

Fig. 1 (a) Schematic illustration of the ring-opening reaction from CHD to HT. (b) Stereochemical two-reaction pathways in CHD. (c) Correlation diagram of the C–C σ bonding/antibonding orbitals and four π orbitals of CHD and the six π orbitals of HT *via* the disrotatory pathway and *via* the conrotatory pathway. (d) Ring-opening reaction pathways of CHD excited to the Rydberg states or 2A (left) and 1B states (right).

the symmetry of MOs is classified as S and A with respect to the two-fold axis, and before and after the ring-opening reaction, the symmetry of occupied MOs in the ground state changes from two S and one A to two A and one S. Because the WH rule predicts the conservation of the symmetry of the occupied MOs, one electron should be excited from π_2 (S) to π_3 (A) on CHD. Therefore, the ring-opening reaction of CHD *via* photoexcitation occurs *via* the conrotatory pathway. Consequently, the reaction pathway of the ring-opening reaction depends on the reaction initiation scheme. The WH rule is thus a powerful tool in stereochemistry to predict final products, yet the dynamic nature of molecular symmetry during the chemical reaction has not been examined.

The recent development of ultrafast laser technology has enabled the observation of reaction dynamics on a timescale of femtoseconds to attoseconds. The reaction dynamics of CHD has been investigated using various spectroscopic techniques[6–25] and theoretical approaches.[26–32] Followed by the excitation to the S_1 (1B) state, the configurational coordinate diagram shown in the right panel of Fig. 1d, is generally accepted as the major ring-opening process.[20,25,31] Upon photoexcitation to the S_1 (1B) state in the Franck–Condon (FC) region, the molecular structure starts distorting, and the S_1 (1B) state is transformed into the S_1 (2A) state accordingly, wherein the potential energy surface has a conical intersection with that of the S_0 (1A) ground state of CHD. At the conical intersection, the electronic state bifurcates into CHD and ring-opened HT. Here, the WH rule predicts that the reaction will follow the conrotatory pathway. By contrast, photoexcitation to the S_2 (2A) or Rydberg states[26,31] is possible by one-photon transition at 6.2 eV[23] or two-photon transition at 3.1 eV.[18,21] The relaxation processes subsequently occur through different pathways shown in the left panel of Fig. 1d, wherein the S_2 (2A) or Rydberg states directly relax to the vibrationally excited states in the ground state of CHD[21,33] followed by the ring-opening reaction from the hot ground state of CHD.[21,23] This ring-opening process is thermally driven; thus the reaction is expected to follow the disrotatory pathway according to the WH rule. However, these two reaction pathways have never been identified on the femtosecond timescale so far, posing a question of the preferred pathway, that is, the conrotatory or disrotatory. Recently, ultrafast electron diffraction has enabled the observation of the real-space dynamics during the photo-induced ring-opening reaction of a CHD derivative, α-phellandrene.[34]

In contrast to this, we investigate the thermal ring-opening reaction of CHD using soft X-ray transient absorption spectroscopy (SX-TAS) at the carbon K-edge and develop a theory to simulate time-dependent molecular structures and the associated near edge X-ray absorption fine structure (NEXAFS) to understand the observed absorption change during the reaction. Because the NEXAFS provides information not only about the atomic species but also about local coordination and bonding between the atoms present in a molecule, we have unique opportunities to gain insight into the bonding states of carbon atoms[35] by SX-TAS. Therefore, the ring-opening processes stimulated by photoexcitation to the 1B state in CHD have already been investigated using SX-TAS,[20] where the relaxation time from the FC state to the conical intersection, shown in Fig. 1d, is 60 ± 20 fs and the subsequent decay is 110 ± 60 fs. However, the reaction pathway in terms of the WH rule has not been explicitly identified. In this study, we demonstrate for the first time that the thermal ring-opening reaction of CHD follows the disrotatory pathway on the femtosecond timescale.

2. Experimental details

We employed a BiB_3O_6-based optical parametric chirped-pulse amplifier (OPCPA) operating at 1.6 μm with a pulse duration of

~10 fs and a repetition rate of 1 kHz, to produce HHG pulses in the soft X-ray.[36] The 3.1 eV pump pulses were obtained from the second-harmonic generation of a Ti:sapphire laser used for pumping the OPCPA. For the probe, a soft X-ray continuum in the range of 200–380 eV was generated by focusing 1.6 μm laser pulses into a Ne-filled gas cell for HHG. More details of the laser system and the experimental setup for SX-TAS are described in ref. 36 and 37, 38, respectively. The CHD samples were purchased from Kanto Chemical Co. and used without further purification. Gaseous CHD molecules at 296 K were filled in a cell with two holes for optical transmittance. The pump and probe pulses were non-collinearly focused on the gas cell. The intensity of the pump pulse was set at 6×10^{12} W cm^{-2}. The transmitted soft X-ray spectra were then recorded with a spectrometer consisting of a slit, a 150 nm-thick aluminum filter, a flat-field grating (Shimadzu 30-003, 2400 grooves per mm), and an X-ray charge-coupled device camera (ANDOR Newton SO). The transient absorption spectra were measured as a function of the delay time between the 3.1 eV pump and the soft X-ray probe pulses. The transient absorption spectra are shown as a change (ΔA) in the absorbance (A). The light intensity after sample gas transmission $I_0 = 10^{-A}$ was changed to $I = 10^{-A-\Delta A}$ by an optical pump. Experimentally, ΔA is obtained from $\Delta A = -\log(I/I_0)$. The fluctuation in ΔA is mainly caused by the probe light. Hence, the experimental error of ΔA was determined to be $\pm 1.0 \times 10^{-3}$ for a bandwidth of 0.05 eV based on the fluctuation at 278 eV, where no photo-induced signals appeared.

The spectrometer was calibrated using the $L_{2,3}$ absorption lines of argon atoms around 250 eV.[39,40] The cross-correlation between the pump and probe pulses was determined from the AC Stark shift of the $2p_{3/2} \rightarrow 3d$ absorption line of argon atoms. The spectrogram of the AC Stark shift and temporal evolution of ΔA is shown in Fig. S1 in the ESI.† Least-squares fitting to the Gaussian function yielded a full width at half maximum of 72 ± 15 fs, which corresponded to the effective temporal resolution of the setup. In this study, although the system could deliver stable attosecond pulses under appropriate operation,[41] the carrier-envelope phase (CEP) of the amplified pulses was not fixed, and the timing and temporal structure of the high harmonic pulses fluctuated. Because the temporal width of the cross-correlation without CEP stabilization 72 ± 15 fs is considerably longer than the timing jitter of the HHG by 1.6 μm, ~10 fs laser pulses, the timing jitter does not degrade the temporal resolution.

The relaxation time τ_1 in the observed process, which will be discussed later, was obtained by least-squares fitting of the data to the exponential function $I(t) = \exp(-t/\tau_1) + C$, convolved with the correlation function $R(t) = \exp\{-4 \ln 2(t/\tau_{FWHM})^2\}$, where t denotes the time and the effective temporal resolution τ_{FWHM} = 72 fs is determined from the AC Stark shift. The constant value C is an offset of the observed signal. The fitting function $f(t)$ is then expressed as follows:

$$f(t) = A\int_{-\infty}^{t} R(t')I(t-t')\mathrm{d}t', \quad (1)$$

where A denotes the amplitude of absorption change.

3. Computational details

The intrinsic reaction coordinates (IRCs) between CHD and HT in the ground state (the S_0 state) were explored using the double-sphere artificial force induced reaction (DS-AFIR) method[42] at the B3LYP-D3/cc-pVDZ level of theory using GRRM17[42] and Gaussian16[43] program packages.

The excitation energies and oscillator strengths of the core excitation spectra were calculated using time-dependent density functional theory (TDDFT) under the Tamm–Dancoff approximation (TDA). By referring to a prior theoretical assessment,[44] Becke's half-and-half exchange and Lee–Yang–Parr correlation (BHHLYP) functional and the correlation-consistent polarized core-valence (cc-pCVDZ) basis set were employed. The TDDFT calculations were performed based on the spin-restricted (closed-shell) Kohn–Sham method for the lowest 1800 excited singlet states (0–300 eV) for neutral states and the spin-unrestricted (open-shell) Kohn–Sham method for the lowest 3500 excited states (0–300 eV) for cationic states, using the Gaussian16[43] program package.

4. Experimental results

Fig. 2a depicts the experimental absorption spectra of CHD in a gas phase. The absorption peak at 284.4 eV (peak X) represents the transition from the carbon 1s orbital to the π* orbital, and the relatively broad absorption peak at ~287.5 eV (peak Y) represents the transition to the σ* orbital.[20,35] Fig. 2b and 2c depict the ΔA spectrogram induced by photoexcitation and the transient ΔA spectra at the designated delay times, respectively.

Fig. 3 shows the temporal evolutions of ΔA at the designated probe photon energies in Fig. 2c by the dotted lines. The energy bandwidths for integration in region I (282.0 eV) were ±0.8 eV. The other bandwidths in regions II (283.8 eV), III (284.6 eV), IV (285.0 eV) and V (285.3 eV) were ±0.3 eV.

Four features can be observed from the absorption changes depicted in Fig. 2b and c. The first feature is the induced absorption around 282.0 eV, which persisted for longer than 1 ps, as shown in the panel I of Fig. 3. The solid line is the fitting result, showing that the induced absorption rose with the temporal resolution of the system (~72 fs). We ascribe these absorption changes to the three-photon ionization of CHD molecules by the pump pulses, because the vertical ionization energy of CHD is 8.25 eV[18] while the excitation photon energy is 3.1 eV. The transition energy from the 1s orbital to the vacant π orbital in the cations is expected to be lower than the energy of the peak X, which will be confirmed theoretically later. Similar spectral changes were observed for a benzene cation,[45,46] which has a transition energy of ~281 eV from the 1s orbital to a partially occupied π-subshell. As shown in the panels II and V of Fig. 3, induced absorption changes upon photoexcitation were also observed up to 1 ps around 283.5 and 285.5 eV, respectively. The theoretical calculation reveals that this also arises from the CHD cation, which will be discussed later. Under the present experimental conditions, several CHD molecules could be ionized, although the pump

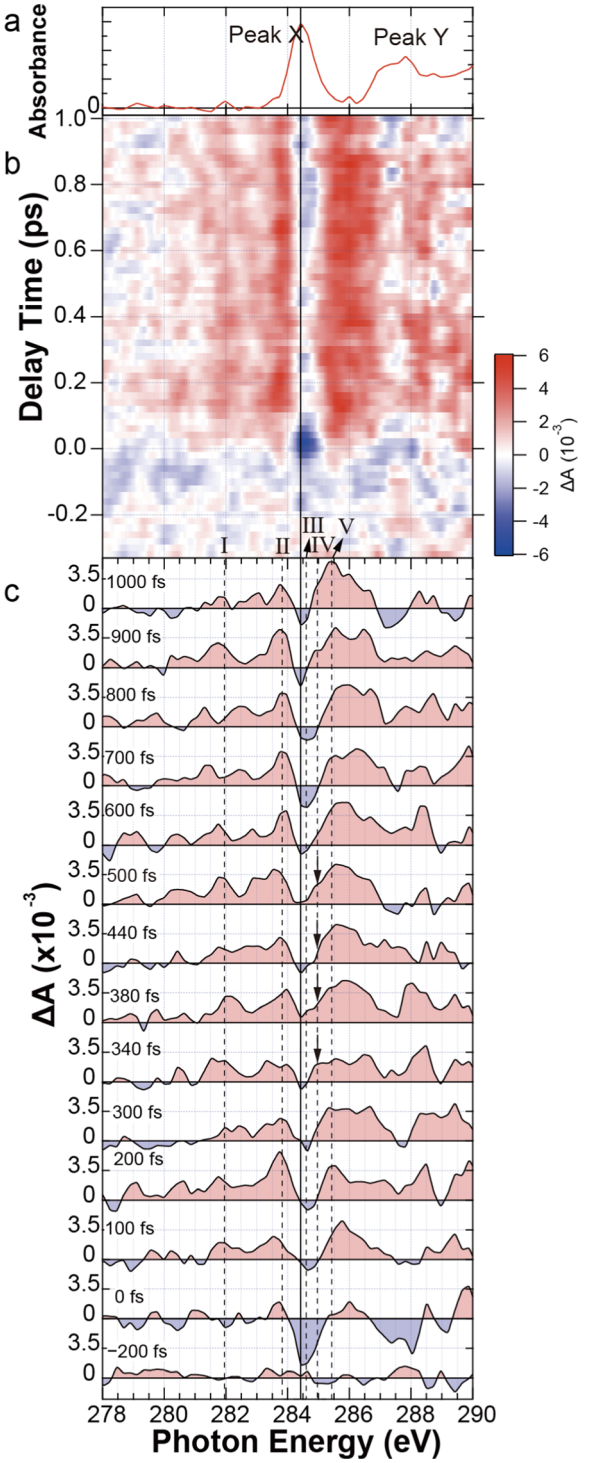

Fig. 2 (a) Stationary absorption spectrum of CHD. (b) ΔA spectrogram. (c) Time-resolved ΔA absorption spectra. The solid vertical line indicates the transition energy from the 1s orbital of a carbon atom to an unoccupied π^* orbital. The dotted lines indicate the photon energies at which the temporal evolutions are plotted in Fig. 3. The arrows indicate the appearance of the shoulders in the valley at 340, 380, 440, and 500 fs.

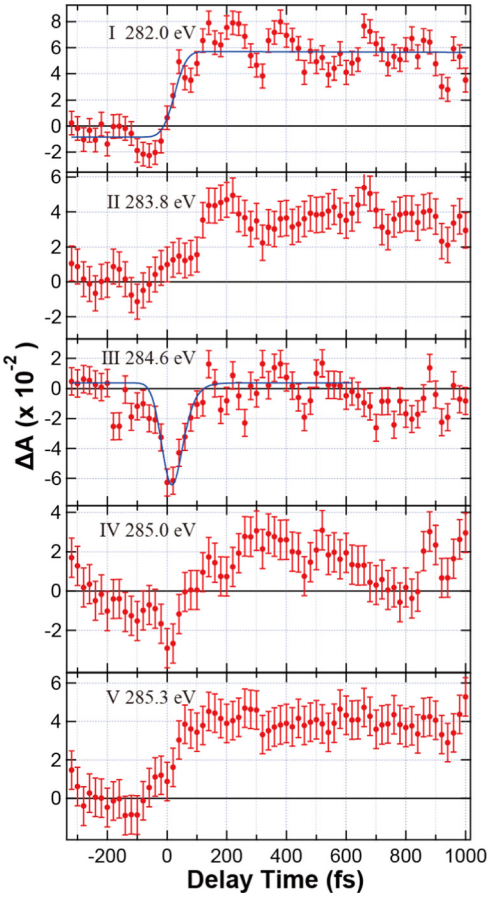

Fig. 3 Temporal evolutions of the absorption changes at I (282.0 eV), II (283.8 eV), III (284.6 eV), IV (285.0 eV), and V (285.3 eV) displayed using dotted lines in Fig. 2c.

intensity (6×10^{12} W cm^{-2}) was set as low as possible to minimize the nonlinear absorption signals while retaining the absorption change ΔA to be observable. Such an experimental condition was necessary to increase the interaction volume of CHD for improving the signal-to-noise ratio, which was inevitable in detection of the multiphoton ionization signals produced at the center of the pump beam.

The second feature is the bleaching of the peak X around 0 fs, which appears in the panel III of Fig. 3. Although a HOMO electron was not directly excited to the π^* orbital, the electronic structure of CHD was modulated by photoexcitation, and accordingly, the peak X was bleached. However, the bleaching of the peak X decreased within 200 fs because of the relaxation from the excited state. The lifetime of the excited Rydberg states was 26 ± 7 fs, obtained by least-squares fitting to a single exponential function convolved with the response time of the system (~72 fs). The fitting result corresponds to the solid line in the panel III. This lifetime is consistent with the lifetime of the excited state measured by time-resolved photoelectron spectroscopy (TR-PES) (37 ± 13 fs).[18] Considering the previous investigations,[18,21,23] we confirm that the ultrafast relaxation to the ground state occurs within 200 fs. Such a fast relaxation time implies that a large excitation energy of 6.2 eV is rapidly shared among the vibrational modes by intramolecular vibrational energy redistribution (IVR) in the ground state of CHD. Energy transfer to the vibrational modes is thus expected to

broaden the absorption lines of the peak X, which remain up to 1 ps. Additionally, the CHD cation also contributes to the bleaching of the peak X. The above consideration of spectral broadening of the peak X and ionization can also explain the feature that the ΔA spectrum in Fig. 2c resembles a valley around the peak X after the relaxation to the ground state of CHD at 200 fs.

The third feature is the temporal evolution of the valley between 300 and 600 fs at $\sim$285 eV. In Fig. 2b and c, the valley around the peak X becomes shallower than that at an earlier timing of $\sim$200 fs. To quantify the dynamics, the temporal evolution of the zero-crossing points of the valley is plotted in Fig. 4c, where its definition is shown in the inset. Here, the energy at the bottom of the valley is used when the bottom of the valley becomes positive and there are no zero-crossing points. Although the amount of energy shifts of the lower zero-crossing point (○) was less than $\pm$0.1 eV after 300 fs, the higher zero-crossing point (□) shifted to the lower side by 0.8 eV between 340 and 600 fs. This relatively large energy shift of the higher zero-crossing point suggests that a new absorption band appeared on the higher energy side of the valley. Fig. 2c shows

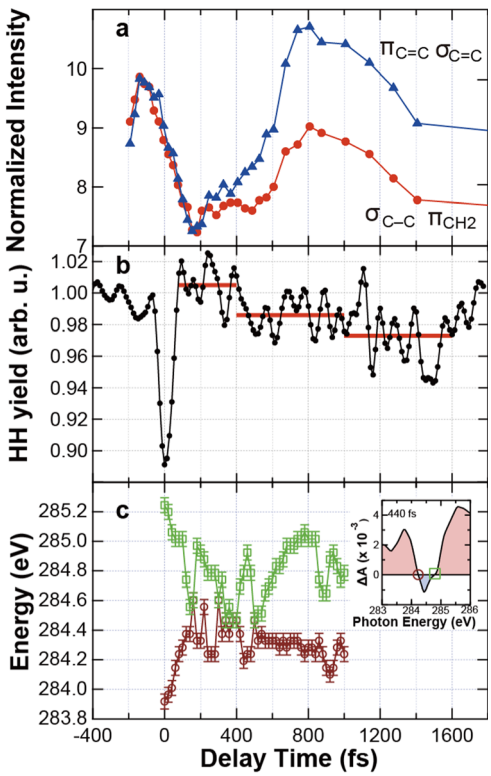

Fig. 4 Temporal evolutions of the experimental signals observed by TR-PES, TR-HHS, and SX-TAS. (a) Time dependence of the photoelectron yields from the MOs related to the C–C and CH_2 bonds of CHD (▲) and with the C=C bond (●) (replot of Fig. 4(c) in ref. 18 with permission from the Royal Society of Chemistry). (b) Time dependence of the yield of the 19th harmonic from CHD (replot of Fig. 3(d) in ref. 21 with permission from the Optical Society of America). (c) Time dependence of the zero-crossing point of the valley in the ΔA spectra. The zero-crossing points are defined in the inset, which is the ΔA spectrum at 440 fs extracted from Fig. 2c. The larger and smaller points are indicated by □ and by ○, respectively.

that ΔA around 285 eV increased between 340 and 600 fs, resulting in a shoulder-like spectrum, which is indicated by the arrows. The temporal evolution of ΔA at the shoulder (285.0 eV) is shown in panel IV of Fig. 3, showing that ΔA values were enhanced between 200 and 700 fs, whereas the temporal evolution in the other spectral regions was almost constant after photoexcitation. The appearance of the absorption around 285.0 eV is the direct evidence for the change in the bonding state.

To highlight the consistency of the results with previous studies,[18,21] the data of TR-PES and time-resolved high harmonic spectroscopy (TR-HHS) upon photoexcitation to the Rydberg states are shown in Fig. 4a and 4b, respectively. TR-PES measures the occupied states including the HOMO by dipole coupling to the continuum while TR-HHS signals reflect the structure and symmetry of the HOMO because of the selective nature of tunnelling. These two methods show the dynamics being more related to the valence electrons, while SX-TAS is more focused on the valence holes probed by core electrons. These three experimental methods thus enable to elucidate the ring-opening dynamics from different viewpoints.

Fig. 4a shows the time dependence of the photoelectron yields from the molecular orbitals related to the C–C and CH_2 bonds (▲) and the C=C bond (●).[18] The experimental spectra are shown in Fig. S2 in the ESI.† The photoelectron yields of the two bands deviate around 400 fs, suggesting the isomerization of CHD.[18] Fig. 4b shows the temporal evolution of the 19th harmonic yield from gaseous CHD observed by TR-HHS. At zero delay time, CHD is excited by two-photon absorption of 400 nm photons to the Rydberg states. The red bars indicate the average values of the data points within the range of the length of each red line. The transient vibrational spectra, shown in Fig. S3 (ESI†), were deduced using a short-time Fourier transform of the harmonic yield. At 400 fs and 1 ps, the harmonic yield and the vibrational spectra changed, which suggests that isomerization occurred at the boundaries between the red horizontal lines and the harmonic yield decreased due to the change in the ionization energy of the isomers.[21]

Another common feature is the ultrafast relaxation from the FC state to the ground state of CHD. As described already, in TR-PES[18] and SX-TAS experiments, the relaxation dynamics with a time constant of $\sim$30 fs were observed. In TR-HHS, the HHG intensity is recovered within 100 fs, suggesting the repopulation of the ground state of CHD. In the TR-PES experiment,[18] we ascribed this ultrafast dynamics to the relaxation from the FC to lower-lying excited states. However, considering the ultrafast dynamics of bleaching in SX-TAS and the ultrafast recovery of the harmonic yield less than 100 fs in TR-HHS shown in Fig. 4b, it is more reasonable to ascribe the observed dynamics to the relaxation to the highly vibrational states in the ground state of CHD.

It is also worth mentioning that PES and HHS probe only the neutral molecules, although the pump pulses could also ionize CHD under the experimental conditions. Because the cation has different ionization energy from the neutral species and because the efficiency of HHG from the cation is drastically

decreased compared to that from the neutral species due to the lower probability of tunnelling ionization, the observed dynamics reflects that of the neutral species. Interestingly, at approximately 400 and 800 fs, all the signals obtained from the three different experimental methods show significant irreversible changes. Therefore, it is concluded that the dynamics in the neutral species was also observed in SX-TAS. The CHD molecule starts isomerizing after approximately 400 fs, although the reaction pathway is still undistinguishable.

Finally, after 600 fs, the shoulder around 285.0 eV in the ΔA spectra disappeared, and hence, the zero-crossing points of the valley shifted to a higher energy (see Fig. 4c). At 840 fs, the zero-crossing energies of the valley shifted again. These results suggest that the molecules were not in a stable state, even after 800 fs. The shifts beyond 800 fs are also consistent with the dynamics observed by TR-PES and TR-HHS presented in Fig. 4a and 4b, respectively. The TR-PES signal showed a decrease in the photoelectron yield beyond 800 fs, while the TR-HHS signal showed that the vibrational spectra varied at approximately 1 ps.[21]

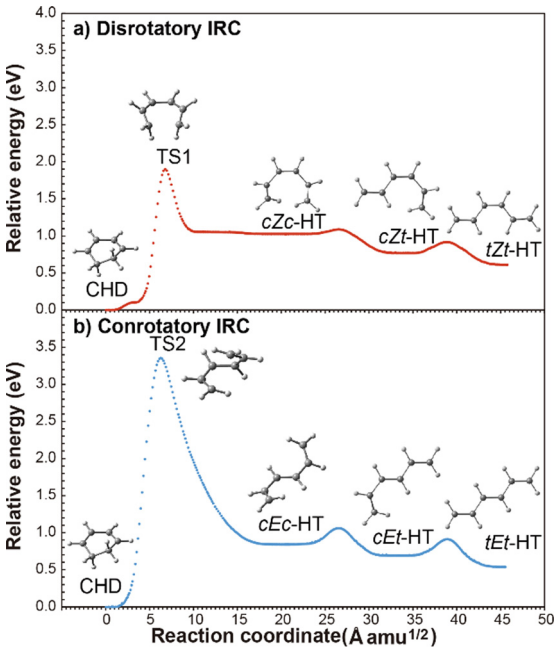

Fig. 5 (a) and (b) Relative energies along the intrinsic reaction coordinates (IRCs) of the disrotatory and conrotatory pathways, respectively. The molecular structures show the key structures of CHD, transition states (TS1 and TS2), and reaction products (*cZc*-, *cZt*-, and *tZt*-HT in the disrotatory path and *cEc*-, *cEt*-, and *tEt*-HT in the conrotatory path) in the ground state.

5. Discussion

5.1 Thermal reaction pathway from a computational approach

To understand the spectral dynamics observed by SX-TAS and to gain insight from the viewpoint of the WH rule, we theoretically investigated the ΔA spectra as follows: under the present excitation conditions, the ring-opening reaction occurs through a thermal process.[21,33] Therefore, the intrinsic reaction coordinates (IRCs) between CHD and HT were explored in the ground state. Two ring-opening pathways, the disrotatory and conrotatory pathways, were identified as shown in Fig. 5a and b, respectively. TS1 and TS2 are the transition states (TSs) of the ring-opening processes on the respective IRCs. The disrotatory and conrotatory IRCs lead to several isomers labelled *cZc*-, *cZt*-, *tZt*-HT and *cEc*-, *cEt*-, *tEt*-HT, respectively. The WH rule predicts that ring-opening in the thermal process follows the disrotatory pathway, which is more consistent with the lower activation barrier of the disrotatory pathway (1.90 eV) than the activation barrier of the conrotatory pathway (3.36 eV), as shown in Fig. 5. Here, a CHD molecule is excited by two 3.1 eV photons and is therefore in highly excited vibrational states after relaxation to the electronic ground state. Hence, although the reaction does not necessarily proceed along the IRCs, it is evident that the disrotatory pathway has the lowest activation barrier. Thus, even when a molecule has a large amount of vibrational energy, the disrotatory IRC is expected to be one of the main reaction channels.

5.2 Theoretical near K-edge absorption

The left panels of Fig. 6 are enlarged views of Fig. 5a and b. Using the computed values, the absorption spectrum at each IRC indicated by a dot in Fig. 6a and b was simulated as follows: first, the bandwidths of absorption lines and the energy scaling factor were determined so as to reproduce the static absorption spectrum of CHD shown in Fig. 2a, where (i) each oscillator has a Gaussian profile with spectral widths of 0.934 and of 1.556 eV below and above 286.5 eV, respectively, and (ii) the energy scale is reduced by multiplication with 0.778. The theoretical spectrum (blue dotted) is shown in Fig. 7a together with the experimental absorption spectrum (red) in Fig. 2a. Then, the ΔA spectra at the designated points on the IRCs in Fig. 6a and b were simulated by employing the same bandwidths and scaling factor. The results are shown in Fig. 6c and d along the disrotatory and conrotatory pathways, respectively.

Here, we would like to point out that the characteristics of the transient spectra around 285 eV may allow the identification of reaction pathways. For the chemical reaction with an activation barrier between a reactant and products, it has been considered challenging to observe TSs experimentally, because the molecular structure changes so rapidly around the TS region. Certainly, at the points before reaching the TSs shown in Fig. 6c and d, the ΔA spectra change so rapidly that it would be difficult to take snapshots of the transient states, while the final products *cZc*-HT and *cEc*-HT (shown by green points and curves in Fig. 6) are observable because they are stable isomers. Between these two regions, the ΔA spectra have similar shapes for long IRCs, specifically between TS1 and point *k* in the disrotatory pathway and between point *j* and *cEc*-HT in the conrotatory pathway. In the case of the Diels–Alder reaction, which is also a kind of pericyclic reactions, a time of 50–150 fs

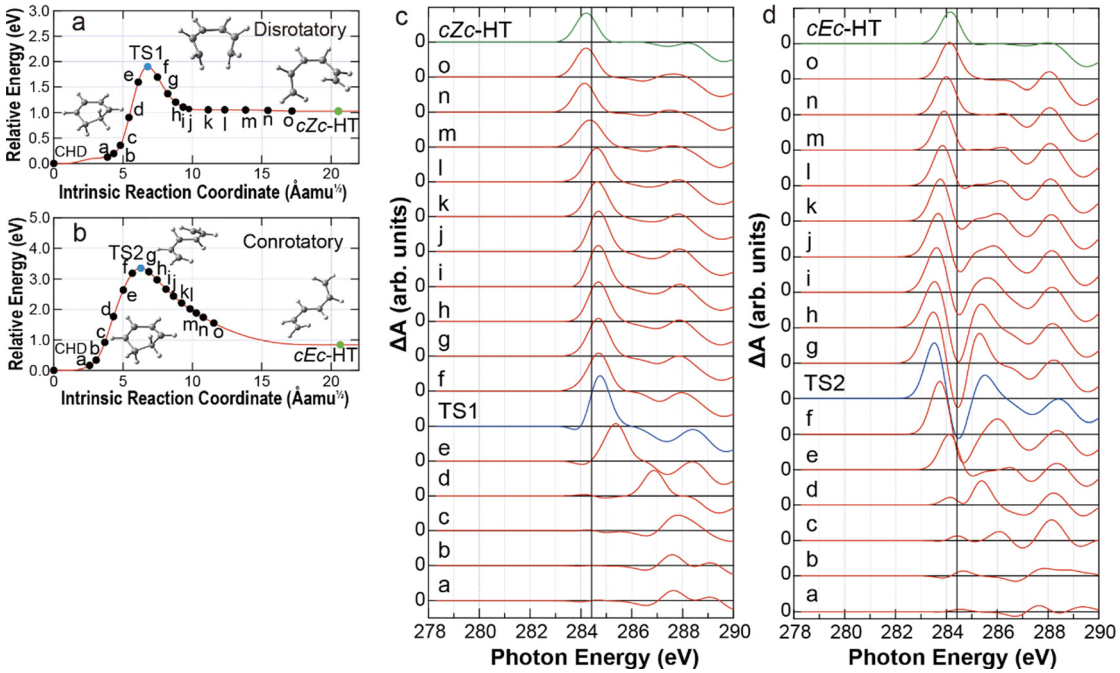

Fig. 6 (a) and (b) IRC points, where Δ*A* spectra are simulated, on the disrotatory and conrotatory energy curves, respectively. (c) and (d) Simulated Δ*A* spectra at the designated points on the IRC along the (a) disrotatory and (b) conrotatory pathways, respectively. The solid vertical lines indicate the energy of peak X.

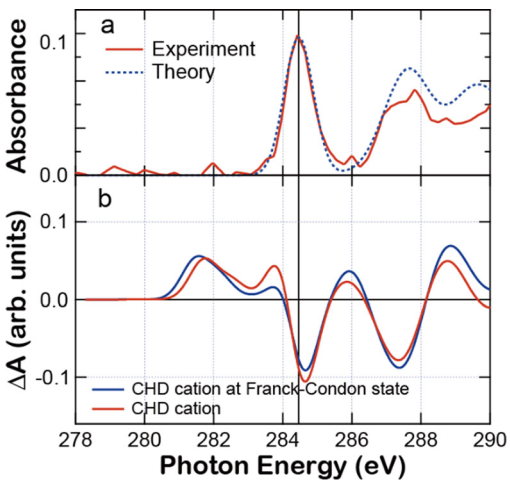

Fig. 7 (a) Experimental (red line) and theoretical (blue dotted line) absorption spectra of CHD. (b) Theoretical Δ*A* spectra of the cation for the Franck–Codon (FC) (blue) and ground states (red). The solid vertical line indicates the energy of peak X.

on average is required for traversing the transition zone.[27] Hence, taking account of the temporal resolution of the system 72 fs, it should be possible to capture the transient states located in the intermediate region.

The theoretical simulation shown in Fig. 6c and d predicts that the peak of the induced absorption in the disrotatory pathway stays around 285.0 eV between TS1 and point *k*, which is higher than peak X (284.4 eV, 1s-π*). On the other hand, in the conrotatory pathway, it remains at a lower transition energy around 284 eV prior to *cEc*-HT shown in Fig. 6d. Hence, the Δ*A* spectrum around peak X could be used to identify the ring-opening direction. As has already been described as the third experimental feature, the transient state appears in the higher energy region compared to peak X between 340 and 600 fs (see Fig. 2c). This experimental feature suggests that the reaction follows the disrotatory pathway. Such energy shifts are attributed to the change of the C–C σ* orbital into π* orbital with the C–C bond cleavage. More detailed computed absorption spectra are shown in the ESI† (Fig. S4 and S5), which are consistent with our interpretation.

Here, we would like to discuss the direction of the energy shift of peak X along the IRCs. The list of calculated excited states of the five key structures (CHD, TS1, *cZc*-HT, TS2, and *cEc*-HT) in the region of peak X is provided in Table S4 (ESI†), and the related MOs and their orbital energy levels are shown in Figs. S6 and S7 (ESI†), respectively (see the ESI†). Peak X of CHD can be assigned to the C_{1s} → LUMO (23*a*) excitation. At TS1 on the disrotatory pathway, the absorption band is found to be high-energy shifted due to the contribution of excitation to LUMO+1 (24*a*) and the low-energy shift of the core orbitals (C_{1s} orbitals). In contrast, for TS2 on the conrotatory pathway, the LUMO (23*a*) energy is very low compared to those of CHD and other structures, indicating that the absorption band is shifted to lower energy. The lower energy of the LUMO at TS2 than those of the others is qualitatively explained as follows: in the structure considered here, the linear combinations of the 2p atomic orbitals of C atoms give a pair of HOMO and LUMO. The energy difference between them depends on the strength of the interaction between the 2p orbitals, which becomes larger with

the degree of overlap between the 2p orbitals. Among these five structures, only TS2 has a non-planar geometry (see Fig. S6, ESI†) and, therefore, the interaction between the 2p orbitals is weaker than in the others. Hence, the LUMO energy of TS2 does not change so much from the energy of the 2p orbitals, while those of the others are shifted to higher. Consequently, the transition energy of $C_{1s} \rightarrow$ LUMO at TS2 along the conrotatory pathway becomes lower than that at TS1 along the disrotatory pathway.

The theoretical investigation also reveals that the first experimental feature observed at around 282 eV (see Fig. 2c) is attributable to the cations as follows: the absorption spectra of cations are simulated using the oscillator strengths of the cations (see Fig. S8, ESI†) with the same bandwidths and energy scaling factor being used for the neutral species. The simulated ΔA spectra of the cations in the ground (red) and FC states (blue) are shown in Fig. 7b. The simulated spectra reproduce the induced absorption around 282 eV, which is the transition to the vacant π orbital in the cation. The bleaching of peak X and the induced absorption around 283.8 and 285.9 eV experimentally observed could also be attributed to the contribution of the cations.

Another finding in the simulated ΔA spectra of the cations shown in Fig. 7b is that the peaks of the induced absorption by the cations stay at around 283.8, 284.7 and 285.9 eV both in the ground and in the FC state. Because the CHD cations retain the ring structures, the structural relaxation from the FC to relaxed structure in the cations does not change the electronic states so much and does not explain the appearance of the transient state observed between 340 and 600 fs. This reinforces that the observed dynamics is due to the neutral molecules.

5.3 Reaction processes

In the previous subsection, it was found that some experimental features in the time-dependent ΔA spectra could be explained by the theoretical calculations of ΔA along IRCs. Here, we will show how the experimentally observed spectra ΔA are correlated to theoretically calculated ΔA spectra by taking into account these features.

The reaction process shown in Fig. 1d can be divided into three steps: relaxation to the ground state up to 200 fs, ring-opening process between 340 and 600 fs, and post-ring-opening process beyond 600 fs. Fig. 8 shows the simulated spectra at each step (blue) along with the experimental ΔA spectra (red).

In the first step at 200 fs, the CHD molecules are in highly vibrationally excited states after relaxation to the electronic ground state of CHD, and some of them are ionized. Hence, the experimental ΔA spectrum at 200 fs shown in red in Fig. 8 consists of (i) the spectral broadening of CHD caused by absorption of a high-energy photon and of (ii) bleaching and induced absorption by ionization. The theoretical simulation qualitatively reproduces the experimental ΔA spectrum shown in blue at the bottom of Fig. 8 with an assumption that 10% of CHD is ionized and that the spectral width of the remaining neutral CHD becomes broader from 0.934 to 1.089 eV.

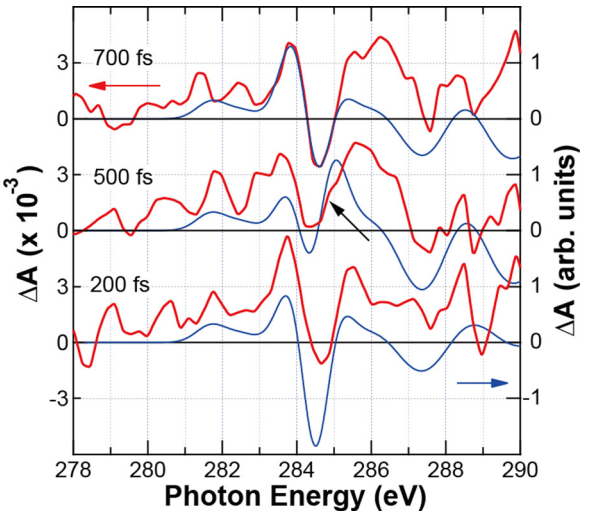

Fig. 8 Theoretical (blue) and experimental (red) ΔA spectra at 200 (bottom), 500 (middle), and 700 fs (top). The black arrow indicates the absorption by the transient state in the disrotatory pathway.

In the second step, a new state at 285.0 eV was found as the third experimental feature. Taking account of the theoretical ΔA spectra shown in Fig. 6c and d, the disrotatory pathway better explains the feature of the second step, because the structures in the conrotatory pathway have the absorption energy lower than peak X at around 284 eV as discussed in Section 5.2. In the present simulation, we assume that the ΔA spectrum of point *f* in Fig. 6a is observable during the reaction. The ΔA spectrum was simulated with an assumption that 20% of the excited molecules proceed to the ring-opening pathway. In addition to the transient state at point *f*, the CHD cation and spectral broadening of the hot CHD were considered. The simulated ΔA spectrum is shown in the middle of Fig. 8 along with the experimental ΔA spectrum at 500 fs. In contrast with the spectrum in the first step, a shoulder on the higher energy side of the valley from the transient states appears, which is indicated by the black arrow. Consequently, we confirm that the excited CHD molecules proceed to the disrotatory pathway between 340 and 600 fs.

In the third step, *i.e.*, after the ring-opening, the ΔA spectra of *cZc*-HT and vibrationally excited hot CHD were included for simulation with the same quantum yields in the second step. The topmost theoretical ΔA spectrum (blue) in Fig. 8 reproduces the experimental spectrum at 700 fs (red). Fig. 4c shows that the higher zero-crossing point of the valley shifted to a higher value owing to the isomerization to *cZc*-HT, which has almost the same absorption energy as CHD. However, at 900 and 1000 fs, the higher zero-crossing point of the valley shifted to lower values again. These features are caused by the isomerization dynamics of HT among *cZc*-, *tZt*-, *tZc*-HT, and so on,[9] because the molecule is still in vibrationally hot states even after ring-opening. TR-PES and TR-HHS exhibited further dynamics after 800 fs as shown in Fig. 4.[18,21]

Finally, we would like to remark about the results obtained by X-ray scattering, where CHD was excited to Rydberg states

with 200 nm light.[23] As mentioned in ref. 23, the diffraction intensities monotonically change up to approximately 600 fs upon photoexcitation, which is attributed to the relaxation to the CHD ground state and the ring-opening reaction to HT with a time constant of 208 ± 11 fs. In contrast, TR-PES, TR-HHS, and SX-TAS resolve more complicated dynamics: the first and second processes are completed by approximately 800 fs. In particular, the first process occurs with a time constant of 26 ± 7 fs and completes within 200 fs (see Fig. 3). This fast process is not separately observed by X-ray scattering. One possible explanation for this is that the differential cross-sections of X-ray scattering in the ground and excited states are similar, and that X-ray diffraction is not necessarily sensitive to the electronic states of CHD in comparison with TR-PES, TR-HHS, and SX-TAS.[47] Therefore, it is crucial to apply various experimental methods to trace chemical reaction dynamics for understanding from different viewpoints.

6. Conclusions

We investigated the thermal ring-opening reaction of CHD using SX-TAS. The thermal reaction is driven by the photoexcitation to the Rydberg states, subsequently followed by ultrafast relaxation to the ground state with a time constant of 26 ± 7 fs. SX-TAS revealed three-step dynamics of the ring-opening reaction: (i) ultrafast relaxation to the ground state of CHD, (ii) isomerization *via* the disrotatory pathway between 340 and 600 fs, which is identified from the spectral changes of the carbon K-edge absorption peculiar to the disrotatory pathway, and (iii) further transformation among HT isomers. This three-step dynamics is consistent with the results obtained from TR-PES[18] and TR-HHS.[21] These approaches detect ultrafast chemical reactions in less than 1 ps with good sensitivity. Among them, the shift of the carbon K-edge absorption observed using SX-TAS can be a sensitive indicator to distinguish steric structures of molecules, enabling the verification of the WH rule on the femtosecond timescale. SX-TAS provides us unique opportunity to investigate chemical reactions.

Author contributions

T. S. and N. S. conceived the project. N. S., N. I., T. M., T. K., J. I., and T. S. designed experiments and T. S., N. S. and Y. K. performed experiments. K. S. and T. T. performed quantum chemical calculations. T. S. analysed the results. T. S., J. I., K. S. and T. T. contributed to discussion and the preparation of the manuscript.

Conflicts of interest

There are no conflicts to declare.

Acknowledgements

T. S. and J. I. were funded by MEXT Q-LEAP (JPMXS0118068681). T. S. was funded by JST CREST (JPMJCR15N1) and KAKENHI (19H01814). J. I. was funded by KAKENHI (18H05250). K. S. and T. T. were funded by JST CREST (JPMJCR1902) and the Photo-Excitonix Project in Hokkaido University. N. I. was funded by JST PRESTO (JPMJPR2002) and KAKENHI (19H02623). T. M. was funded by KAKENHI (20K05358). Some of the calculations were performed using the Research Centre for Computational Science, Okazaki, Japan (project: 22-IMS-C019).

References

1 C. M. Beaudry, J. P. Malerich and D. Trauner, *Chem. Rev.*, 2005, **105**, 4757–4778.
2 S. Deb and P. M. Weber, *Annu. Rev. Phys. Chem.*, 2011, **62**, 19–39.
3 B. C. Arruda and R. J. Sension, *Phys. Chem. Chem. Phys.*, 2014, **16**, 4439–4455.
4 J. E. Baldwin and S. M. Krueger, *J. Am. Chem. Soc.*, 1969, **91**, 6444–6447.
5 R. B. Woodward and R. Hoffmann, *Angew. Chem., Int. Ed. Engl.*, 1969, **8**, 781–853.
6 R. McDiarmid, A. Sabljić and J. P. Doering, *J. Chem. Phys.*, 1985, **83**, 2147–2152.
7 S. A. Trushin, W. Fuß, T. Schikarski, W. E. Schmid and K. L. Kompa, *J. Chem. Phys.*, 1997, **106**, 9386–9389.
8 W. Fuß, W. E. Schmid and S. A. Trushin, *J. Chem. Phys.*, 2000, **112**, 8347–8362.
9 C.-Y. Ruan, V. A. Lobastov, R. Srinivasan, B. M. Goodson, H. Ihee and A. H. Zewail, *Proc. Natl. Acad. Sci. U. S. A.*, 2001, **98**, 7117–7122.
10 N. Kuthirummal, F. M. Rudakov, C. L. Evans and P. M. Weber, *J. Chem. Phys.*, 2006, **125**, 133307.
11 K. Kosma, S. A. Trushin, W. Fuß and W. E. Schmid, *Phys. Chem. Chem. Phys.*, 2009, **11**, 172–181.
12 J. L. White, J. Kim, V. S. Petrovi and P. H. Bucksbaum, *J. Chem. Phys.*, 2012, **136**, 054303.
13 V. S. Petrović, M. Siano, J. L. White, N. Berrah, C. Bostedt, J. D. Bozek, D. Broege, M. Chalfin, R. N. Coffee, J. Cryan, L. Fang, J. P. Farrell, L. J. Frasinski, J. M. Glownia, M. Gühr, M. Hoener, D. M. P. Holland, J. Kim, J. P. Marangos, T. Martinez, B. K. McFarland, R. S. Minns, S. Miyabe, S. Schorb, R. J. Sension, L. S. Spector, R. Squibb, H. Tao, J. G. Underwood and P. H. Bucksbaum, *Phys. Rev. Lett.*, 2012, **108**, 253006.
14 V. S. Petrovic, S. Schorb, J. Kim, J. White, J. P. Cryan, J. M. Glownia, L. Zipp, D. Broege, S. Miyabe, H. Tao, T. Martinez and P. H. Bucksbaum, *J. Chem. Phys.*, 2013, **139**, 184309.
15 S. Adachi, M. Sato and T. Suzuki, *J. Phys. Chem. Lett.*, 2015, **6**, 343–346.
16 C. C. Pemberton, Y. Zhang, K. Saita, A. Kirrander and P. M. Weber, *J. Phys. Chem. A*, 2015, **119**, 8832–8845.
17 M. P. Minitti, J. M. Budarz, A. Kirrander, J. S. Robinson, D. Ratner, T. J. Lane, D. Zhu, J. M. Glownia, M. Kozina, H. T. Lemke, M. Sikorski, Y. Feng, S. Nelson, K. Saita, B. Stankus, T. Northey, J. B. Hastings and P. M. Weber, *Phys. Rev. Lett.*, 2015, **114**, 255501.
18 R. Iikubo, T. Sekikawa, Y. Harabuchi and T. Taketsugu, *Faraday Discuss.*, 2016, **194**, 147–160.

19 O. Schalk, T. Geng, T. Thompson, N. Baluyot, R. D. Thomas, E. Tapavicza and T. Hansson, *J. Phys. Chem. A*, 2016, **120**, 2320–2329.
20 A. R. Attar, A. Bhattacherjee, C. D. Pemmaraju, K. Schnorr, K. D. Closser, D. Prendergast and S. R. Leone, *Science*, 2017, **356**, 54–59.
21 K. Kaneshima, Y. Ninota and T. Sekikawa, *Opt. Express*, 2018, **26**, 31039–31054.
22 T. J. A. Wolf, D. M. Sanchez, J. Yang, R. M. Parrish, J. P. F. Nunes, M. Centurion, R. Coffee, J. P. Cryan, M. Gühr, K. Hegazy, A. Kirrander, R. K. Li, J. Ruddock, X. Shen, T. Vecchione, S. P. Weathersby, P. M. Weber, K. Wilkin, H. Yong, Q. Zheng, X. J. Wang, M. P. Minitti and T. J. Martínez, *Nat. Chem.*, 2019, **11**, 504–509.
23 J. M. Ruddock, H. Yong, B. Stankus, W. Du, N. Goff, Y. Chang, A. Odate, A. M. Carrascosa, D. Bellshaw, N. Zotev, M. Liang, S. Carbajo, J. Koglin, J. S. Robinson, S. Boutet, A. Kirrander, M. P. Minitti and P. M. Weber, *Sci. Adv.*, 2019, **5**, eaax6625.
24 K. Kaneshima, Y. Ninota and T. Sekikawa, *J. Opt. Soc. Am. B*, 2021, **38**, 441–447.
25 S. Karashima, A. Humeniuk, R. Uenishi, T. Horio, M. Kanno, T. Ohta, J. Nishitani, R. Mitrić and T. Suzuki, *J. Am. Chem. Soc.*, 2021, **143**, 8034–8045.
26 M. Merchán, L. Serrano-Andrés, L. S. Slater, B. O. Roos, R. McDiarmid and X. Xing, *J. Phys. Chem. A*, 1999, **103**, 5468–5476.
27 K. Black, P. Liu, L. Xu, C. Doubleday and K. N. Houk, *Proc. Natl. Acad. Sci. U. S. A.*, 2012, **109**, 12860–12865.
28 M. Garavelli, C. S. Page, P. Celani, M. Olivucci, W. E. Schmid, S. A. Trushin and W. Fuss, *J. Phys. Chem. A*, 2001, **105**, 4458–4469.
29 H. Tamura, S. Nanbu, T. Ishida and H. Nakamura, *J. Chem. Phys.*, 2006, **124**, 084313.
30 A. Nenov, P. Kolle, M. A. Robb and R. D. Vivie-Riedle, *J. Org. Chem.*, 2010, **75**, 123–129.
31 I. Polyak, L. Hutton, R. Crespo-Otero, M. Barbatti and P. J. Knowles, *J. Chem. Theory Comput.*, 2019, **15**, 3929–3940.
32 M. Filatov, S. K. Min and K. S. Kim, *Mol. Phys.*, 2019, **117**, 1128–1141.
33 C. C. Bühler, M. P. Minitti, S. Deb, J. Bao and P. M. Weber, *J. At., Mol., Opt. Phys.*, 2011, **2011**, 637593.
34 E. G. Champenois, D. M. Sanchez, J. Yang, J. P. F. Nunes, A. Attar, M. Centurion, R. Forbes, M. Gühr, K. Hegazy, F. Ji, S. K. Saha, Y. Liu, M.-F. Lin, D. Luo, B. Moore, X. Shen, M. R. Ware, X. J. Wang, T. J. Martínez and T. J. A. Wolf, *Science*, 2021, **374**, 178–182.
35 C. Kolczewski, R. Püttner, M. Martins, A. S. Schlachter, G. Snell, M. M. Sant'Anna, K. Hermann and G. Kaindl, *J. Chem. Phys.*, 2006, **12**, 15607.
36 N. Ishii, K. Kaneshima, K. Kitano, T. Kanai, S. Watanabe and J. Itatani, *Nat. Commun.*, 2014, **5**, 3331.
37 N. Saito, H. Sannohe, N. Ishii, T. Kanai, N. Kosugi, Y. Wu, A. Chew, S. Han, Z. Chang and J. Itatani, *Optica*, 2019, **6**, 1542–1546.
38 N. Saito, N. Douguet, H. Sannohe, N. Ishii, T. Kanai, Y. Wu, A. Chew, S. Han, B. I. Schneider, J. Olsen, L. Argenti, Z. Chang and J. Itatani, *Phys. Rev. Res.*, 2021, **3**, 043222.
39 G. Jabbari, T. Miteva, V. Stumpf, K. Gokhberg, P. O'Keeffe, A. Ciavardini, P. Bolognesi, M. Coreno, L. Avaldi, E. Keshavarz, M. Ghandehari, M. Tozihi, C. Callegari, M. Alagia, K. C. Prince, A. Kivimäkig and R. Richter, *Phys. Chem. Chem. Phys.*, 2015, **17**, 22160–22169.
40 O. Schwarzkopf, F. Eggenstein, U. Flechsig, C. Kalus, H. Lammert, U. Menthel, G. Reichardt, P. Rotter, F. Senf, T. Zeschke and W. B. Peatman, *Rev. Sci. Instrum.*, 1998, **69**, 3789–3793.
41 N. Saito, N. Ishii, T. Kanai, S. Watanabe and J. Itatani, *Sci. Rep.*, 2016, **6**, 35594.
42 S. Maeda, Y. Harabuchi, M. Takagi, K. Saita, K. Suzuki, T. Ichino, Y. Sumiya, K. Sugiyama and Y. Ono, *J. Comput. Chem.*, 2018, **39**, 233–251.
43 M. J. Frisch, G. W. Trucks, H. B. Schlegel, G. E. Scuseria, M. A. Robb, J. R. Cheeseman, G. Scalmani, V. Barone, G. A. Petersson, H. Nakatsuji, M. C. X. Li, A. V. Marenich, J. Bloino, B. G. Janesko, R. Gomperts, B. Mennucci, H. P. Hratchian, J. V. Ortiz, A. F. Izmaylov, J. L. Sonnenberg, D. Williams-Young, F. Ding, F. Lipparini, F. Egidi, J. Goings, B. Peng, A. Petrone, T. Henderson, D. Ranasinghe, V. G. Zakrzewski, J. Gao, N. Rega, G. Zheng, W. Liang, M. Hada, M. Ehara, K. Toyota, R. Fukuda, J. Hasegawa, M. Ishida, T. Nakajima, Y. Honda, O. Kitao, H. Nakai, T. Vreven, K. Throssell, J. J. A. Montgomery, J. E. Peralta, F. Ogliaro, M. J. Bearpark, J. J. Heyd, E. N. Brothers, K. N. Kudin, V. N. Staroverov, T. A. Keith, R. Kobayashi, J. Normand, K. Raghavachari, A. P. Rendell, J. C. Burant, S. S. Iyengar, J. Tomasi, M. Cossi, J. M. Millam, M. Klene, C. Adamo, R. Cammi, J. W. Ochterski, R. L. Martin, K. Morokuma, O. Farkas, J. B. Foresman and D. J. Fox, *Gaussian 16, Revision B.01*, Gaussian, Inc., Wallingford CT, 2016.
44 A. Nakata, Y. Imamura, T. Otsuka and H. Nakai, *J. Chem. Phys.*, 2006, **124**, 094105.
45 M. Epshtein, V. Scutelnic, Z. Yang, T. Xue, M. L. Vidal, A. I. Krylov, S. Coriani and S. R. Leone, *J. Phys. Chem. A*, 2020, **124**, 9524–9531.
46 M. L. Vidal, M. Epshtein, V. Scutelnic, Z. Yang, T. Xue, S. R. Leone, A. I. Krylov and S. Coriani, *J. Phys. Chem. A*, 2020, **124**, 9532–9541.
47 Y. Liu, S. L. Horton, J. Yang, J. P. F. Nunes, X. Shen, T. J. A. Wolf, R. Forbes, C. Cheng, B. Moore, M. Centurion, K. Hegazy, R. Li, M.-F. Lin, A. Stolow, P. Hockett, T. Rozgonyi, P. Marquetand, X. Wang and T. Weinacht, *Phys. Rev. X*, 2020, **10**, 021016.

